Biogeosciences Discuss., 12, 3101–3143, 2015
www.biogeosciences-discuss.net/12/3101/2015/
doi:10.5194/bgd-12-3101-2015

Biogeosciences Discussions
Open Access

Global soil nitrous oxide emissions in a dynamic carbon–nitrogen model

Y. Y. Huang and S. Gerber

Soil and Water Science Department, Institute of Food and Agricultural Sciences, University of Florida, Gainesville, Florida 32611, USA

Received: 23 December 2014 – Accepted: 16 January 2015 – Published: 11 February 2015

Correspondence to: S. Gerber (sgerber@ufl.edu)

Published by Copernicus Publications on behalf of the European Geosciences Union.

Abstract

Nitrous oxide (N_2O) is an important greenhouse gas that also contributes to the depletion of stratospheric ozone. With high temporal and spatial heterogeneity, a quantitative understanding of terrestrial N_2O emission, its variabilities and reponses to climate change is challenging. We added a soil N_2O emission module to the dynamic global land model LM3V-N, and tested its sensitivity to soil moisture regime and responses to elevated CO_2 and temperature. The model was capable of reproducing the average of cross-site observed annual mean emissions, although differences remained across individual sites if stand-level measurements were representative of gridcell emissions. Modelled N_2O fluxes were highly sensitive to water filled pore space (WFPS), with a global sensitivity of approximately 0.25 Tg N year^{-1} per 0.01 change in WFPS. We found that the global response of N_2O emission to CO_2 fertilization was largely determined by the response of tropical emissions, whereas the extratropical response was weaker and different, highlighting the need to expand field studies in tropical ecosystems. Warming generally enhanced N_2O efflux, and the enhancement was greatly dampened when combined with elevated CO_2, although CO_2 alone had a small effect. Our analysis suggests caution when extrapolation from current field CO_2 enrichment and warming studies to the global scale.

1 Introduction

Nitrous oxide (N_2O) is a major reactant in depleting stratospheric ozone as well as an important greenhouse gas (Ravishankara et al., 2009; Butterbach-Bahl et al., 2013; Ciais et al., 2013). With a global warming potential of 298 times more (per unit mass) than that of carbon dioxide (CO_2) over a 100 year period (Forster et al., 2007), the contributions of N_2O emissions to global radiative forcing and climate change are of critical concern (Zaehle and Dalmonech, 2011). The concentration of atmospheric N_2O has been increasing considerably since the industrial revolution with a linear rate of

BGD
12, 3101–3143, 2015

0.73 ± 0.03 ppb year^{-1} over the last three decades (Ciais et al., 2013). Although applications of synthetic fertilizer and manure during agriculture intensification have been identified as the major causes of this increase (Davidson, 2009; Zaehle and Dalmonech, 2011), nonagricultural (natural) soil is still an important source that is comparable to the combined anthropogenic emissions (Ciais et al., 2013; Syakila and Kroeze, 2011). N_2O fluxes from nonagricultural soils are highly heterogeneous, which limits our ability to estimate and predict global scale budget, and quantify its response to global environmental changes (Butterbach-Bahl et al., 2013; Ciais et al., 2013).

Most of the N_2O fluxes from soil are produced by microbial nitrification and denitrification (Braker and Conrad, 2011; Syakila and Kroeze, 2011). Nitrification is an aerobic process that oxidizes ammonium (NH_4^+) to nitrate (NO_3^-), during which some N is lost as N_2O. Denitrification reduces nitrate or nitrite to gaseous N (i.e. NO_x, N_2O and N_2), a process that is fostered under anaerobic conditions. N_2O is generated in intermediary steps during denitrification and a small portion can escape from soil before further reduction to N_2 takes place. Soil texture, soil NH_4^+, soil water filled pore space (WFPS), mineralization rate, soil pH, and soil temperature are well-known regulators of nitrification N_2O fluxes (Parton et al., 1996, 2001; Li et al., 2000). Denitrification and associated N_2O emissions depend primarily on carbon supply, the redox potential and soil NO_3^- (Firestone and Davidson, 1989; Parton et al., 1996). Soil moisture has a particular strong impact (Galloway et al., 2003; Schlesinger, 2009) as it influences nitrification and denitrification rates through its regulations on substrate availability and soil redox potential (as oxgyen diffusion proceeds at much slower rate in water filled than in air filled pore space), thereby also controlling the partitioning among various denitrification products (i.e. NO_x, N_2O and N_2) (Firestone and Davidson, 1989; Parton et al., 2001). Although emissions are known to be sensitive to soil moisture, quantitative understanding of its role in terrestrial N_2O fluxes and variability is limited (Ciais et al., 2013).

At regional to global scale, the application of the "hole-in-pipe" concept (Firestone and Davidson, 1989) in the CASA biosphere model pioneered one of the earliest

BGD
12, 3101–3143, 2015

process-based estimation of natural soil N_2O fluxes. The model calculated the sum of NO, N_2O and N_2 fluxes as a constant portion of gross mineralized N, and the relative ratios of N trace gases ($NO_x : N_2O : N_2$) as a function of soil moisture (Potter et al., 1996). While the early models of nitrification and denitrification are primarily conceptual driven, recent global N_2O models combine advancements in global dynamic land models with more detailed processes, including microbial dynamics. Xu and Prentice (2008) simplified nitrification and denitrification modules from DNDC (i.e., DeNitrification–DeComposition) (Li et al., 1992, 2000) in their global scale dynamic N scheme (DyN) and incorporated DyN into the LPJ dynamic global vegetation model. In the DNDC approach, nitrification and denitrification were allowed to happen simultaneously in aerobic and anaerobic microsites. Zaehle et al. (2011) incorporated a nitrification–denitrification scheme into the O–CN land model following largely the LPJ-DyN with minor modifications and additions of the effects of soil pH and chemo-denitrification that originated from DNDC (Li et al., 2000). Compared to LPJ-DyN approach, Saikawa et al. (2013) retained the explicit simulation of nitrifying and denitrifying bacteria from DNDC in their CLMCN-N2O module based on CLM V3.5 land model. Simulations with LPJ-DyN and O–CN demonstrated a positive response of N_2O emissions to historical warming and a negative response to historical CO_2 increase, globally. This negative CO_2 response seems to be in disagreement with one meta-analysis of manipulative field experiments showing an increase in N_2O emissions at elevated levels of CO_2 (Zaehle et al., 2011; Xu et al., 2012; van Groenigen et al., 2011). The discrepancy in response to global change factors needs to be addressed both in models and in the interpretation of manipulative field experiments.

Here we add a N_2O gas emission module to LM3V-N, a land model developed at the Gephysical Fluid Dynamics Laboratory (GFDL). In this paper, we will first describe the added N_2O emission module. We then subject the model to historic changes in CO_2, N deposition, and recent climate change to infer natural N_2O emissions in the past few decades. We test the model's sensitivity to soil water regime, by addressing the parameterization of soil WFPS, and by data-overriding of two different soil moisture re-

BGD
12, 3101–3143, 2015

analysis products. We then subject the model to step changes in atmospheric CO_2 and temperature to understand modelled reponses to CO_2 fertilization and climate change.

2 Methods

2.1 Model description

LM3V is capable of simulating ecosystem dynamics and exchange of CO_2, water and energy between land and atmosphere with the fastest time step of 30 min (Shevliakova et al., 2009). LM3V-N expands the LM3V land model with a prognostic N cycle (Gerber et al., 2010). The model includes five plant functional types (PFTs): C3 and C4 grasses, tropical, temperate deciduous and cold evergreen trees. Each PFT has five vegetation C pools (leaves, fine roots, sapwood, labile, and wood), two litter and two soil organic C pools and their corresponding N pools based on the specific C : N ratios. Photosynthesis is coupled with stomatal conductance on the basis of the Collatz et al. (1991, 1992) simplification of the Farquhar scheme (Farquhar et al., 1980). N enters the ecosystem through atmospheric N deposition and biological N fixation (BNF). BNF in LM3V-N is dynamically simulated on the basis of plant N availability, N demand and light condition.

Organic matter decomposition is based on a modified CENTURY approach (Bolker et al., 1998), and amended with formulation of N dependent C and N mineralization rates. The fate of soil mineral N (i.e. ammonium and nitrate) depends on the relative strength of the competing sinks, with the hierarchy order of soil immobilization > plant uptake > leaching/denitrification. Denitrification thus far is lumped with leaching losses and summed into a generic N loss term. Over the long term, losses of N from fire and dissolved organic nitrogen (DON) are critical factors limiting the ecosystem N accumulation and maintaining N limitation in LM3V-N (Gerber et al., 2010, 2013). Soil hydrology in LM3V follows partly on Land Dynamics (LaD) with further improvements (Shevliakova et al., 2009; Milly and Shmakin, 2002; Milly et al., 2014).

BGD
12, 3101–3143, 2015

Here, we add a soil nitrification–denitrification module which accounts for N gaseous losses from NH_3 volatilization, nitrification and denitrification. The nitrification–denitrification scheme implemented here combines features from both the DNDC model (Li et al., 1992, 2000) and the CENTURY/DAYCENT (Parton et al., 1996, 2001; Del Grosso et al., 2000). Details of model formulation and implementation are given in Appendix A. Briefly, nitrification is treated as a donor (NH_4^+) controlled process which is further modified by soil moisture and temperature. Denitrification, a multiple step process that anaerobically reduces nitrate sequentially to the endproduct N_2, is simplified as a single process controlled by substrate NO_3^- (electron acceptor), labile C availability (electron donor), soil moisture and temperature. Heterotropical respiration (HR) is used as a surrogate for labile C availability, similar to Del Grosso et al. (2000) and Xu and Prentice (2008). WFPS plays a crucial role in the prediction of nitrification an denitrification, as it determines movement of dissolved molecules, and more importantly, puts strong constraints on movement of oxygen in soils, affecting the soil's redox potential. We therefore use WFPS to parameterize the soil's redox potential and substrate availability to nitrifying and denitrifying microbes.

N_2O is released as a byproduct from both nitrification and denitrification. The fraction of N_2O lost from net nitrification is uncertain (Li et al., 2000; Xu and Prentice, 2008). Here we set this fraction to be 0.4 %, which is higher than Goodroad and Keeney (1984), but at the low end provided by Khalil et al. (2004). Gaseous losses from denitrification is partitioned among N gas species (i.e. NO_x, N_2O and N_2) on the basis of $NO_x : N_2O$ ratio ($R_{NO_x:N_2O}$) (Parton et al., 2001) and $N_2 : N_2O$ ratio ($R_{N_2:N_2O}$) (Del Grosso et al., 2000). $R_{NO_x:N_2O}$ varies with gas diffusivity (Parton et al., 2001), which is estimated from air filled porosity (Davidson and Trumbore, 1995). $R_{N_2:N_2O}$ combines the effects of substrate (NO_3^-) to electron donor ratio and WFPS (Del Grosso et al., 2000).

BGD
12, 3101–3143, 2015

2.2 Model experiments

2.2.1 Global hindcast with potential vegetation

To understand the model performance and compare with other models and observations, we conducted a hindcast simulation with potential vegetation. The model resolution was set to 3.75° longitude by 2.5° latitude. We forced the model with 3 hourly reanalysis weather data based on Sheffield et al. (2006). We used a 17 year recycled climate of 1948–1964 for the spin-up and simulation years prior to 1948. Atmospheric CO_2 concentration was prescribed with 284 ppm for model spin-up and based on ice core and atmospheric measurements for transient simulations (Keeling et al., 2009). N deposition was set as natural background for simulations before 1850 (Dentener and Crutzen, 1994), and interpolated linearly between the natural background and a snapshot of contemporary (1995) deposition (Dentener et al., 2006) for simulations after 1850. Soil pH was prescribed and derived from the Harmonized World Soil Database (HWSD) version 1.1, the same as NACP model driver data (Wei et al., 2014).

The model was spun up from bare ground without C–N interactions for the first 68 years and with C–N interactions for the following 1200 years to develop and equilibrate C and N stocks. During spin-up, slow litter C and slow soil C and N pools were set to the equilibrium values based on litterfall inputs and decomposition/leaching rates every 17 years. We determined the model to reach a quasi-equlibrium state by confirming the drift to be less than 0.03 $Pg\,C\,year^{-1}$ for global C storage and 0.2 $Tg\,N\,year^{-1}$ for global N storage. From this quasi equilibrium state, we initialized the global hindcast experiment from 1850 using the corresponding climatic forcings, CO_2 and N deposition data. In the analysis, we will focus on the last three decades (1970–2005) when most of the data are available.

BGD
12, 3101–3143, 2015

2.2.2 Sensitivity to soil water filled pore space (WFPS)

While LM3V-N carries a simplified hydrology, we bracketed effects of soil moisture by exploring the paremeterization of WFPS and by substituting the predicted soil moisture with 3 hourly re-analysis data. Levels of soil water (in units kg m^{-2}) therefore stem from: (1) the simulated water content based on LM3V-N soil water module, hereafter LM3V-SM (2) the Global Land Data Assimilation System Version 2 with the land surface model NOAH 3.3 (Rodell et al., 2004), hereafter NOAH-SM, and (3) the ERA Interim reanalysis dataset from European Center for Medium range Weather Forecasting (ECMWF) (Dee et al., 2011), hereafter ERA-SM. The latter two datasets integrate satellite and ground based obervations with land surface models. When overriding soil moisture, we linearly interpolated the 3 hourly data onto the 30 min model time step. In these simulations, we allowed soil C and N dynamics to vary according to different soil moisture datasets, but kept the model prediction of soil water to use for plant productivity and evapotranspiration.

Parameterization of the soil moisture effect on nitrification and denitrification are based on WFPS. LM3V-N uses the concept of plant available water, where the maximum amount of water a soil can hold varies between the wilting point and field capacity (Milly and Shmakin, 2002). To test the effect of WFPS on N_2O emissions, we calcuated WFPS using three methods. Method 1 assumes WFPS is the ratio of available water and the available water capacity in the rooting zone. In method 2 we assume, WFPS is the ratio of the water filled porosity and total porosity which is derived from bulk density (BD). BD was obtained from the Harmonized World Soil Database (HWSD) version 1.1 (Wei et al., 2014). The calculation is given by

$$\mathrm{WFPS} = \frac{\frac{\theta}{h_r} \times 0.001}{1 - \frac{\mathrm{BD}}{2.65}} \quad (1)$$

where θ (kg m^{-2}) is the root zone soil water; h_r (m) is the effective rooting depth of vegetation. Method 1 leads generally to an overestimation of WFPS with the available

BGD
12, 3101–3143, 2015

water capacity smaller than total pore space. In contrast, the use of method 2 with LM3V-SM creates an underestimation since water is not allowed to accumulate beyond field capacity and misses high WFPS to which nitrification and denitrification are sensitive. Meanwhile, for NOAH-SM and ERA-SM, Methods 2 are more close to the "real" WFPS. In a third approach, which is also the default method applied in the global hindcast experiment and the elevated CO_2 and temperature responses experiment, calculates WFPS as the average of the previous two methods.

For each soil moisture dataset (3 in total, 2 replacements and 1 simulated by LM3V-N), we calculated WFPS using three methods mentioned above. We conducted transient simulations with the nine different WFPSs (3 datasets × 3 methods) starting from the near equilibrium state obtained in the global hindcast experiment in Sect. 2.2.1. The simulation procedure was the same as that in global hindcast experiment except for the WFPS. ERA-SM is only availabe starting from 1979, prior to which simulations were conducted with model default soil moisture (LM3V-SM).

2.2.3 Responses to elevated CO_2 and temperature

The respones of N_2O emissions to atmospheric CO_2 and global warming have been intensively studied at field scale. Here, we evaluate the model's response to a doubling of preindustrial CO_2 level (284 to 568 ppm) and a 2 K increase in atmospheric temperature. Starting from the quasi-equalibrium state with potential vegetation obtained in global hindcast experiment in Sect. 2.2.1, we conducted four transient model runs: (1) the CONTROL run with the same drivers as spin-up, (2) the CO2_FERT run with the same drivers as the CONTROL except a doubling of atmospheric CO_2 level, (3) the TEMP run with the same drivers as the CONTROL except a 2 K rise in atmospheric temperature, and (4) the CO2_FERT × TEMP run with both the doubling of CO_2 and 2 K rise in temperature. For each experiment, we ran the model for 100 years and evaluated the corresponding results.

BGD
12, 3101–3143, 2015

2.3 Comparisons with observations and correlations with environmental variables

We compared our model results for annual N_2O gas loss with field data: we compiled annual N_2O emissions from peer-reviewed literature (see Appendix B for more information). To increase the representativeness of the measurements, we included only sites with more than 3 months or 100 days experimental span. We limited our datasets where there was no reference to a disturbance of any kind. Only locations with at least 50 years non-disturbance history for forests and 10 years for vegetation other than forests were included. The compiled 61 measurements cover a variety of spatial ranges with vegetation types including tropical rainforest, temperate forest, boreal forest, tundra, savanna, perennial grass, steppe, alpine grass and desert vegetation. Multiple measurements falling into the same model grid cell were averaged. If the authors had indicated the dominant vegetation or soil type, we used the values reported for the dominant type instead of the averaged. For multiyear measurements, even if the authors gave the individual year's data, we averaged the data to avoid overweighting of long term studies. If the location was between borders of different model grid cells, we averaged across the neighboring grid cells.

Pearson correlation coefficient with the significance threshold of $\alpha < 0.05$ was used to quantify the correlation between N_2O fluxes and environmental variables, i.e. soil temperature, root zone water content, gross primary productivity, net mineralization rate, soil ammonium and soil nitrate content, for each grid cell from the global hindcast run.

BGD
12, 3101–3143, 2015

3 Results

3.1 Global budget, seasonal and inter-annual variability

Our modelled global soil N_2O flux is $6.82 \pm 0.28\,Tg\,N\,year^{-1}$ (1970–2005 mean and SD) (Fig. 1) which is within the range of reported values: the central estimation of N_2O emission from soils under natural vegetation is $6.6\,Tg\,N\,year^{-1}$ based on the Intergovernmental Panel on Climate Change (IPCC) AR5 (Ciais et al., 2013) (range, 3.3–9.0 $Tg\,N\,year^{-1}$) for the mid-1990s. Mean estimation for the period of 1975–2000 ranged from 7.4 to $10.6\,Tg\,N\,year^{-1}$ with different precipitation forcing data (Saikawa et al., 2013). Xu et al. (2012) reported the decadal-average to be 8.3–10.3 $Tg\,N\,year^{-1}$ for the 20th century. Potter and Klooster (1998) reported a global mean emission rate of $9.7\,Tg\,N\,year^{-1}$ over 1983–1988, which is higher than the earlier version of their model ($6.1\,Tg\,N\,year^{-1}$) (Potter et al., 1996). Other estimates includes 6–7 $Tg\,N\,year^{-1}$ (Syakila and Kroeze, 2011), $6.8\,Tg\,N\,year^{-1}$ based on the O–CN model (Zaehle et al., 2011), 3.9–6.5 $Tg\,N\,year^{-1}$ for preindustrial periods from a top-down inversion study (Hirsch et al., 2006), 1.96–4.56 $Tg\,N\,year^{-1}$ in 2000 extrapolated from field measurements by an artificial neural network approach (Zhuang et al., 2012), 6.6–7.0 $Tg\,N\,year^{-1}$ for 1990 (Bouwman et al., 1995), and 7–16 $Tg\,N\,year^{-1}$ (Bowden, 1986) as well as 3–25 $Tg\,N\,year^{-1}$ (Banin, 1986) from two earlier studies.

Following Thompson et al. (2014), El Niño years are set to the years with the multivariate ENSO index (MEI) greater than 0.6. 1972, 1977, 1982, 1983, 1987, 1991, 1992, 1993, 1994, 1997 and 1998 were chosen as El Niño years. We detected reduced emissions during El Niño years (Fig. 1), in line with the global atmospheric inversion study of Thompson et al. (2014) and the process based modelling study from Saikawa et al. (2013).

Figure 2 shows the simulated global natural soil N_2O emissions in 4 seasons averaged over the period of 1970–2005. The Northern Hemisphere displays a large seasonal variability, with the highest emissions in the northern summer (JJA, June to August) and lowest in winter (DJF, December to February). Globally, northern spring

BGD
12, 3101–3143, 2015

(MAM, March to May) has the highest emission rate (2.07 Tg N) followed by summer (1.89 Tg N). The smaller emissions in summer compared to spring stems from a reduced contribution of the Southern Hemisphere during northern summer.

As expected, a large portion (more than 60 %) of the soil N_2O fluxes has tropical origin (23.5° S to 23.5° N), while emissions from cooler regions are limited by temperature and arid/semi-arid regions by soil water. Our modelling results suggested year-round high emission rates from humid zones of Amazonia, east central Africa, and throughout the islands of Southeast Asia, with small seasonal variations (Fig. 2). Emissions from tropical savannah are highly variable, with locations of both high fluxes (seasonal mean $> 90\,mgN\,m^{-2}\,season^{-1}$ or $3.6\,kg\,ha^{-1}\,year^{-1}$) and low fluxes (seasonal mean $< 4\,mgN\,m^{-2}\,season^{-1}$ or $0.16\,kg\,ha^{-1}\,year^{-1}$). The simulated average tropical emission rate is $0.78\,kg\,N\,ha^{-1}\,year^{-1}$ (1970–2005), within the range of estimates ($0.2–1.4\,kg\,N\,ha^{-1}\,year^{-1}$) based on site-level observations from the database of Stehfest and Bouwman (2006), but smaller than a more detailed simulation study ($1.2\,kg\,N\,ha^{-1}\,year^{-1}$) carried out by Werner et al. (2007). Our analysis here excluded land cover, land use changes and human management impacts, while most of the observation-based or regional modelling studies did not factor out those impacts. Our modelling result in natural tropics is comparable with another global modelling study (average emission rate, $0.7\,kg\,N\,ha^{-1}\,year^{-1}$) (Zaehle et al., 2010), in which the authors claimed they might underestimate the tropical N_2O sources compared to the inversion estimates from the atmospheric transport model TM3 (Hirsch et al., 2006).

3.2 Sensitivity to WFPS

Soil N_2O emissions generally increase with WFPS (Fig. 4). WFPS derived from Method 1 is higher than that based on Method 2. Soil moisture datasets and calculation methods together produced a range of 0.15–0.72 for the global mean WFPS (1982–2005). Mean values greater than 0.6 (approximately field capacity) are less realistic, though these high WFPS values provide the opportunity to test the model's sensitivity. Global soil N_2O emissions are highly sensitive to WFPS, with approximately 0.25 Tg N per

BGD
12, 3101–3143, 2015

year per 0.01 change in global mean WFPS in the range 0 to 0.6. The spatial and temporal characteristic of WFPS also matters. With mean WFPS of ca. 0.21 the emission rate from LM3V-SM (Fig. 4 green cycle) is 1.13 Tg N year^{-1} higher than that from NOAH-SM (Fig. 4 blue triangle), showing effects of regional and temporal differences between the soil moisture products.

3.3 Model–observation comparisons

Modelled N_2O emissions capture the cross-site observation mean (0.54 vs. 0.53 kg N ha^{-1} year^{-1} based on LM3V-SM with WFPS Method 3) reasonably at the annual time step (Appendix B and Fig. 3a), but spread considerably along the 1 : 1 line. The points deviating the most are from tropical forests, with overestimations from montane tropical forest and underestimations from lowland tropical forests if those measurements are representative of gridcell emissions. These patterns are similar as results from NOAH-SM (Appendix B and Fig. 3b) and ERA-SM (Appendix B and Fig. 3c) with WFPS based on Method 2, except that the application of WFPS from NOAH-SM slightly underestimates the observed global mean (0.54 vs. 0.47 kg N ha^{-1} year^{-1} from NOAH-SM with WFPS based on Method 2).

3.4 Correlations with environmental variables

Fig. 5 illustrates the temporal correlations between simulated monthly soil N_2O emissions and environmental variables (surface soil temperature, root zone soil water content, gross primary productivity, net mineralization rate, soil ammonium content and soil nitrate content), which were either predicted by the model or model inputs (forcings). The results show, that temperature is a strong driver of N_2O emissions in boreal and across large swaths of temperate regions. Temperature directly affects nitrification and denitrification rates, and also alters the N made available from mineralization and competition with plant uptake. Higher temperature triggers N_2O emissions from boreal and a large fraction of temperate ecosystems, while both positive and negative temperature

BGD
12, 3101–3143, 2015

relationships exist in tropical forests (Fig. 5a). Covariation with soil temperature results in a strong postive link between gross primary productivity, net mineralization rate and N_2O emission in the northern high latitudes (Fig. 5d). Likewise, higher root zone water content is associated with higher soil N_2O emissions except in the northern mid- to high latitudes where soil temperature is the primary controller (Fig. 5a and b). Tropical forests and some of the humid temperate regions with high N_2O emissions show the strongest soil moisture-N_2O flux correlations, which partly explains the high sensitivity of global soil N_2O budget to WFPS.

As expected, N_2O emissions are strongly and positively correlated with soil nitrate content at the global scale (Fig. 5f), while the relationships between N_2O emissions and soil ammonium (Fig. 5e) varies. In the humid tropics, N_2O fluxes are negatively correlated with soil ammonium content. This negative pattern may partly result from the inverse relationship between soil ammnium content and nitrification rate. In our model, soil ammonium content is not only constrained by temperature or moisture but is also subjected to varying biological demand from plants and microbes. For example, high nitrification can draw down ammonium concentration in the soil. Compared to the humid tropics, soil ammonium levels in cold or dry areas appear to be mainly controlled by N supply (mostly from SOM decomposition/N mineralization). In cold (or dry) regions, SOM decomposition/N mineralization, nitrification and denitrification are all regulated by soil temperature (or moisture) (Fig. 5a). The correlation between soil ammonium and N_2O fluxes covaries with the soil temperature (or moisture)–N_2O flux relationship.

3.5 CO_2 and temperature responses

Globally, N_2O emissions respond to a step CO_2 increase first with a decline to ultimately increased levels after approximately 40 years (Fig. 6a, black line). The simulated global response follows largely the behaviour as simulated for tropical forests (Fig. 6a, yellow line). The shift from a negative to a positive response indicates possible competing mechanisms operating on different time scales. Field level experiments revealed

BGD
12, 3101–3143, 2015

the highly variable effects of CO_2 fertilization on N_2O emissions. From meta-analysis, van Groenigen et al. (2011) suggested that elevated CO_2 significantly increased N_2O emission by 18.8 %, while Dijkstra et al. (2012) argued for a non-significant response in non-N-fertilized studies. In contrast to observation studies, two global C–N cycle model analyses suggested negative effects from CO_2 fertilization (Xu et al., 2012; Zaehle et al., 2011). The negative impacts (reduced N_2O flux), which are also reported from manipulative experiments, are likely from increased plant N and immobilization demand under CO_2 fertilization, reducing N availability for nitrifiers and denitrifiers. Positive effects (increase N_2O fluxes) can result from the impacts of elevated CO_2 level to increase litter production and consequently C sources for denitrifiers, and to increase soil moisture from reduced stomatal conductance and leaf transpiration. With both of these positive and negative mechanisms embedded in our model, the net effects depend on the relative strength of those opposing forces.

Temperate deciduous forests, where most of the forest CO_2 fertilization experiments are conducted, respond positively to elevated CO_2 level (Fig. 6a, green line). The slight increase in modelled N_2O emission are comparable with the mean response of field data compiled for temperate forests (ca. 0.01–0.03 $kg\,N\,year^{-1}\,ha^{-1}$) (Dijkstra et al., 2012). A similar positive response was detected for cold evergreen forests (Fig. 6a, pink line) with stronger magnitude compared to temperate deciduous forests. For grasslands, Dijkstra et al. (2012) reported small negative mean response from northern mixed prairie (ΔN_2O, ca. −0.01 to −0.03 $kg\,N\,year^{-1}\,ha^{-1}$), zero mean response from shortgrass steppe and positive mean response from annual grassland (ca. 0.03–0.06 $kg\,N\,year^{-1}\,ha^{-1}$). Our model shows a small negative mean response from C4 grassland (Fig. 6a, cyan line) with the similar magnitude of that reported for the Northern mixed prairie, where the composition of C4 grass varies (Dijkstra et al., 2012). A CO_2 increase in C3 grassland initially reduces N_2O emission (Fig. 6a, blue line). However, this initial slight negative response turns into a small positive response within one decade.

BGD
12, 3101–3143, 2015

Elevated temperature generally increases N_2O emissions except for the slight negative effect in C4 grass (Fig. 6b). Overall the response to a 2 °C warming is bigger than that of doubling of CO_2. The simulated temperature effects are more pronounced in the first decade and decrease over time in tropical forests (Fig. 6b, yellow line), while for the temperate deciduous forests (Fig. 6b, green line) and boreal forests (Fig. 6b pink line), the temperature effects become more pronounced over time. Simulated temperate forest response (in the first decade) is close to that of observed mean (ca. 0.2–0.5 kg N year^{-1} ha^{-1}) (Dijkstra et al., 2012). Our modelled slight negative response in C4 grass and positive in C3 grass are in alignment with data compiled by Dijkstra et al. (2012) who reported both positive and negative responses in grasslands.

The results of combining CO_2 and temperature are similar to the CO_2 effect alone (Fig. 6c), despite the fact, that the individual effect of temperature is much stronger than that of CO_2. This antagonistic interaction (i.e. the combined enhancement in N_2O flux from elevated CO_2 and temperature are smaller than the summary of their individual effects) is also evident for C3 grass (first 50 years), temperate deciduous tree and cold evergreen forests (Fig. 6d).

4 Discussion

Our model combines knowledge from two of the most widely applied biogeochemical models (DNDC and CENTURY) with current advancements in field level studies. Our global model is capable of reproducing the global mean natural N_2O emissions from other modeling and inverse methods, and observed cross-site annual mean behavior. By focusing on the role of soil moisture in N_2O emissions, we find a global scale high dependence of simulated N_2O emissions on soil moisture (WFPS), mainly driven by emissions from tropical regions. The model broadly reproduces the magnitude and direction of responses to elevated CO_2 and temperature from manipulative field experiments where data is available. The global responses to elevated CO_2 and temperature follow largely the response of tropical forests, where a noted absence of field exper-

BGD
12, 3101–3143, 2015

iments exsit. Next, we will further discuss modelled responses to soil moisture and elevated atmospheric CO_2 and temperature.

Evaluation of global simulations agaist field measurements is susceptible to scale mismatches. The complexity of microscale interactions for N_2O production creates notorious large spatial and temporal variabilities which are undoubtedly difficult to constraint even at the stand level (Butterbach-Bahl et al., 2013). The homogeneous representation of environmental drivers within model grid cells casts doubt on site-specific model-observation comparison in global simulations. For example, N_2O emissions vary with topography which are not treated explicitly in most of the global C–N models. 3.8 times difference was detected in a montane forest (Central Sulawesi, Indonesia) moving from 1190 to 1800 m (Purbopuspito et al., 2006), and 4.3 times difference was found from a tropical moist forest (Brazilian Atlantic Forest) with the altitude change from 100 to 1000 m (Sousa Neto et al., 2011). Nevertheless, modeling approaches can offer important insights with respect to scaling our understanding of the mechanism of N_2O gas emissions to the globe.

Soil moisture is a key variable in climate system but difficult to derive or measure at the global scale (Seneviratne et al., 2010). Our modelled fluxes are highly sensitive to WFPS, which is in agreement with observation and model synthesis studies (Heinen, 2006; Butterbach-Bahl et al., 2013). The large range when calculating WFPS from different methods resulted in a difference of more than 5 $Tg\,N\,year^{-1}$ in global soil N_2O fluxes. Saikawa et al. (2013) found an up to 3.5 $Tg\,N\,year^{-1}$ gap induced by different precipitation forcing data from CLMCN-N2O. It is difficult to single out the difference caused by soil moisture alone from their results. Nevertheless, those two studies did suggest the importance of improving the dynamics of soil water for the purpose of predicting soil N_2O emission and climate feedbacks.

The root zone soil water in LM3V-N is based on a single layer bucket model. This simplified treatment of soil water dynamics may increase the difficulty in reproducing the temporal and spatial dynamics of WFPS. As a first step, we used the average between the oringinal analog in LM3V-N and that derived from soil total porosity to

BGD
12, 3101–3143, 2015

account for actual soil moisture and the possibility of soil water above field capacity. Meanwhile, with soil moisture replace treatments (NOAH-SM and ERA-SM), WFPS based on method 2 (total porosity) is more close to real WFPS, indicating that the most realistic soil N_2O emission is in the range of 5.74–7.47 Tg N year^{-1}. A more realistic root zone water module, such as multilayer representations of biogeochemistry and soil water dynamics, would refine models of soil N_2O emissions. El Niño events trigger reduced soil emissions in our results similar as proposed by Saikawa et al. (2013) and Thompson et al. (2014). El Niño events are known to have induced several of the most well known large scale droughts and alters soil moisture dynamics (Schwalm et al., 2011). Tropical forests N_2O emissions are highly correlated with root zone soil water content and contribute strongly to the global-scale fluxes of N_2O in our model. Whether there is a strong link between soil N_2O emission anomalies and El Niño induced soil moisture deviations needs further investigation with improved soil hydrology.

Patterns of seasonality, and the correlates between N_2O emissions vs. temperature and soil moisture suggest that moisture is the dominant driver of N_2O emission in tropical regions and soil temperature critical elsewhere. However, globally, the tropical fluxes contribute with more than 60 % to the global soil N_2O fluxes. Also, the global responses to elevated CO_2 and temperature is dominated by the tropical response. In contrast to temperate and boreal forests, tropical forests respond negatively to elevated CO_2 in the first few decades. Our results therefore suggest caution when extrapolating from current manipulative field studies to the globe: the postive response to CO_2 enrichment as obtained from (mostly) extratropical field study may be overestimated, when the studies' fluxes are scaled up to the globe. Moreover, we found strong interaction of elevated CO_2 and temperature, acting to reduce soil N_2O emission compared to the sum of individual responses, highlighting the non-linear impacts of CO_2 and temperature on N_2O emissions. We realize that this interaction is likely to be different when incorporating other factors (Brown et al., 2012), such as N depostion and land use change (disturbance). In addition, step changes in atmospheric CO_2 and temperature compared to gradual and sustained increases may also lead to differences, and may explain the

BGD
12, 3101–3143, 2015

discrepancy to two of the global modeling studies that suggested an overall positive response of soil N_2O emission to the effects of elevated CO_2 and climate change (Xu et al., 2012; Zaehle et al., 2011). However, step changes mimic most closely manipulative experiments. Nevertheless, the largest uncertainties lie in the tropical region where our model indicated strongest responses and strongest nonlinear interactions of elevated CO_2 and temperature.

In addition to the uncertainties mentioned above, we simplified N_2O sources and processes, ignoring other microbial metabolic pathways and aboitic processes that produce or consume N_2O. The global magnitude of those ignored process remains largely unexplored. We do not incorporate explicit mechanisms for N_2O emissions from freeze–thaw cycle or poorly drained soils (e.g.wetlands), the uptake of organic N etc., which might be globally important, especially with future climate changes. Considering those uncertainties and gaps, more studies are in need in order to unstand the terretrial N_2O emissions.

5 Conclusions

We present estimates of terrestrial soil N_2O fluxes under natural vegetation (1970 to 2005) based on a new N_2O emission module embedded into the global C–N cycle model LM3V-N. To determine the sensitivity of the modelling result to soil water (WFPS), we replaced the root zone soil water with two other derived datasets and altered the way in which WFPS is calculated. Our best estimate of modelled global soil N_2O flux is $6.82 \pm 0.28\,\mathrm{Tg\,N\,year^{-1}}$ (1970–2005 mean and interannual variability), within the range of current understanding of soil N_2O emissions, but highly sensitive to WFPS. Improvement of soil hydrology is likely to significantly reduce the large uncertainties associated with soil N_2O emission estimates. Although the simulated mean responses are in agreement with manipulative field studies where effects of elevated CO_2 and temperature were investigated, we found that the global response was dom-

BGD
12, 3101–3143, 2015

inated by tropical forest, where our model suggest a different response than the field studies carried out in temperate ecosystems.

Appendix A: Soil N_2O emission module

Gaseous losses so far were not differentiated from hydrological leaching in LM3V-N. In this part, we provide details on the nitrification–denitrification module which explicitly simulates N gaseous losses from nitrification and denitrification, as well as other process modifications compared to the original LM3V-N.

A1 Nitrification–Denitrification

Transformation among inorganic N speicies (ammonium and nitrate) occurs mainly through two microbial pathways: nitrification and denitrification. Our simulation of N_2O losses during nitrification–denitrification generally follows the "hole-in-pipe" concept (Firestone and Davidson, 1989) with more detailed treatment of the N flux pipes and the leaky holes (gaseous losses) in the pipes.

Although ongoing debate exists in whether nitrification rates might be well described by bulk soil ammonium concentration or soil N turnover rate (Parton et al., 1996; Zaehle and Dalmonech, 2011), we adopt the donor controlled scheme (ammonium concentration). In additon to substrate, soil texture, soil water filled pore space (WFPS, the percentage of soil pore space filled with water), and soil temperature are all well known regulators of nitrification. As a first order approximation, nitrification rate (N) is simulated as a function of soil temperature, NH_4^+ availability and WFPS,

$$N = k_n f_n(T) f_n(\mathrm{WFPS}) \frac{N_{\mathrm{NH}_4^+}}{b_{N,\mathrm{NH}_4^+}} \quad \text{(A1)}$$

where k_n is the ammonium turnover rate (11 000 year^{-1}, the same as in LM3V-N). b_{N,NH_4^+} is the buffer parameter for NH_4^+ (10 in LM3V-N); $f_n(T)$ is the tempera-

BGD
12, 3101–3143, 2015

ture response function and f_n(WFPS) is the soil water response function following Li et al. (2000), with a optimum temperature for nitrification at 35 °C. The effect of WFPS on nitrification is texture dependent, with most of the reported optimum value around 0.6 (Parton et al., 1996; Linn and Doran, 1984). We adopted the WFPS response function from Parton et al. (1996) with medium soil texture.

$$f_n(T) = \left(\frac{60 - T_{\text{soil}}}{25.78}\right)^{3.503} \times e^{\frac{3.503\times(T_{\text{soil}}-34.22)}{25.78}} \quad \text{(A2)}$$

$$f_n(\text{WFPS}) = \left(\frac{\text{WFPS} - 1.27}{-0.67}\right)^{\frac{1.9028}{0.59988}} \times \left(\frac{\text{WFPS} - 0.0012}{0.59988}\right)^{2.84} \quad \text{(A3)}$$

where T_{soil} is the soil temperature in degree Celsius. Denitrification is controlled by substrate NO_3^- (electron acceptor), labile C availability (electron donor), soil moisture and temperature. The responses of denitrification to substrate and labile C availability follow Michaelis–Menten kinetics. Labile C availability is estimated by soil heterotrophic respiration (HR). Following LPJ-DyN (Xu and Prentice, 2008), denitrification is assumed to have a Q_{10} value of 2 when the soil temperature is between 15 and 25 °C. Soil moisture response function is based on Parton et al. (1996). Soil pH is reported to be an important indicator of chemodenitrification which occurs only in acidic soils (pH < 5) under conditions of high nitrite concentration. However, its role for N_2O production is not well studied (Li et al., 2000) and we do not model the chemodenitrification explicitly.

$$D = f_d(T) f_d(\text{WFPS}) \frac{\text{HR}}{\text{HR} + K_c} \frac{NO_3^-}{NO_3^- + K_n} \quad \text{(A4)}$$

and

$$NO_3^- = \frac{N_{NO_3^-}}{b_{NO_3^-}} \quad \text{(A5)}$$

BGD
12, 3101–3143, 2015

where D is the denitrification, K_c, K_n are Michaelis–Menten constants taken from Li et al. (2000) (0.017 and 0.083 $\mathrm{kg\,N\,m^{-3}}$ respectively); $b_{NO_3^-}$ is the buffer parameter for NO_3^- (1 in LM3V-N); $f_d(T)$ and f_d(WFPS) are soil temperature and water reponse function for denitrification given by the following two equations

$$f_d(T) = e^{308.56\times\left(\frac{1}{68.02}+\frac{1}{T_{soil}+46.02}\right)} \quad \text{(A6)}$$

$$f_d(\mathrm{WFPS}) = \frac{1.56}{12.0^{\left(\frac{16.0}{12.0^{(2.01\times \mathrm{WFPS})}}\right)}} \quad \text{(A7)}$$

A2 Gaseous partitions from nitrification–denitrification

N_2O loss from net nitrification is a constant fraction of 0.4 %. NO_x emission from nitrification is based on the $NO_x : N_2O$ ratio ($R_{NO_x:N_2O}$). $R_{NO_x:N_2O}$ varies with gas diffusivity (D/D_0) (Parton et al., 2001), which is estimated from air filled porosity (AFPS) (Davidson and Trumbore, 1995)

$$R_{NO_x:N_2O} = 15.2 + \frac{35.5 \times \mathrm{ATAN}\left[0.68 \times \pi \times \left(10 \times \frac{D}{D_0} - 1.68\right)\right]}{\pi} \quad \text{(A8)}$$

$$\frac{D}{D_0} = 0.209 \times \mathrm{AFPS}^{\frac{4}{3}} \quad \text{(A9)}$$

where ATAN stands for the trigonometric arctangent function; AFPS is the air filled porosity (1-WFPS), and π is the mathematical constant, approximately 3.14159.

During denitrification, the gaseous ratio between N_2 and N_2O ($R_{N_2:N_2O}$) is calculated following Del Grosso et al. (2000), which combines the effects of substrate (NO_3^-) to electron donor (HR, the proxy for labile C) ratio and WFPS.

$$R_{N_2:N_2O} = \mathrm{Fr}\left(\frac{NO_3^-}{HR}\right) \cdot \mathrm{Fr(WFPS)} \quad \text{(A10)}$$

BGD
12, 3101–3143, 2015

with

$$\mathrm{Fr}\left(\frac{\mathrm{NO_3^-}}{\mathrm{HR}}\right) = \max\left(0.16 \times k, k \times e^{\left(-0.8 \times \frac{\mathrm{NO_3^-}}{\mathrm{HR}}\right)}\right) \quad \text{(A11)}$$

$$\mathrm{Fr(WFPS)} = \max(0.1, 0.015 \times \mathrm{WFPS} - 0.32)$$

where k is a texture dependent parameter (Table A1) estimated from Del Grosso et al. (2000).

A3 Other modified processes

We also added NH_3 volatilization into LM3V-N. NH_3 volatilization in soil results from the difference between the equilibrium NH_3 partial pressure in soil solution and that in the air. Dissolved NH_3 is regulated by ammonium concentration and pH. The net flux of NH_3 from soil to the atmosphere varies with soil NH_3, moisture, temperature, therefore

$$\mathrm{NH_3} = f(\mathrm{pH}) f_{\mathrm{NH_3}}(T)(1 - \mathrm{WFPS}) \frac{N_{\mathrm{NH_4^+}}}{b_{N,\mathrm{NH_4^+}}} \quad \text{(A12)}$$

where NH_3 is the net ammonia volatilization flux from each modelling step; $f(\mathrm{pH})$ is the pH factor and $f(T)$ is the temperature factor which are given by the following two equations

$$f(\mathrm{pH}) = e^{2 \times (\mathrm{pH_{soil}} - 10)} \quad \text{(A13)}$$

$$f_{\mathrm{NH_3}}(T) = \min\left(1, e^{308.56 \times \left(\frac{1}{71.02} - \frac{1}{T_{\mathrm{soil}} + 46.02}\right)}\right) \quad \text{(A14)}$$

where $\mathrm{pH_{soil}}$ is the soil pH which is prescribed instead of simulated dynamically. $f(\mathrm{pH})$ and $f(T)$ follow largely on the NH_3 volatilization scheme implemented in the dynamic global vegetation model LPJ-DyN (Xu and Prentice, 2008).

BGD
12, 3101–3143, 2015

Appendix B: Observed annual N_2O fluxes data

Annual N_2O fluxes data were compiled from peer-reviewed literature. We applied simple selection criteria (see the main text) to reduce the mismatches between model outputs and field measurements, bearing in mind the gaps between complex field conditions and idealized model forcings. Latitutes (Lat) and longitudes (Lon) in Table B1 are based on model grids.

Acknowledgements. The soil moisture data used in this study were acquired as part of the mission of NASA's Earth Science Division and archived and distributed by the Goddard Earth Sciences (GES) Data and Information Services Center (DISC).

References

Ball, T., Smith, K. A., and Moncrieff, J. B.: Effect of stand age on greenhouse gas fluxes from a Sitka spruce [*Picea sitchensis* (Bong.) Carr.] chronosequence on a peaty gley soil, Glob. Change Biol., 13, 2128–2142, doi:10.1111/j.1365-2486.2007.01427.x, 2007.

Banin, A.: Global budget of N_2O: the role of soils and their change, Sci. Total Environ., 55, 27–38, doi:10.1016/0048-9697(86)90166-x, 1986.

Billings, S. A., Schaeffer, S. M., and Evans, R. D.: Trace N gas losses and N mineralization in Mojave desert soils exposed to elevated CO_2, Soil Biol. Biochem., 34, 1777–1784, doi:10.1016/s0038-0717(02)00166-9, 2002.

Bolker, B. M., Pacala, S. W., and Parton, W. J.: Linear analysis of soil decomposition: insights from the century model, Ecol. Appl., 8, 425–439, doi:10.2307/2641082, 1998.

Bouwman, A. F., Vanderhoek, K. W., and Olivier, J. G. J.: Uncertainties in the global source distribution of nitrous oxide, J. Geophys. Res.-Atmos., 100, 2785–2800, doi:10.1029/94jd02946, 1995.

Bowden, R. D., Steudler, P. A., Melillo, J. M., and Aber, J. D.: Annual nitrous-oxide fluxes from temperate forest soils in the northeastern United-States, J. Geophys. Res.-Atmos., 95, 13997–14005, doi:10.1029/JD095iD09p13997, 1990.

BGD
12, 3101–3143, 2015

Bowden, W. B.: Gaseous nitrogen emmissions from undisturbed terrestrial ecosystems: an assessment of their impacts on local and global nitrogen budgets, Biogeochemistry, 2, 249–279, doi:10.1007/bf02180161, 1986.

Braker, G. and Conrad, R.: Diversity, structure, and size of N_2O-producing microbial communities in soils-what matters for their functioning?, in: Advances in Applied Microbiology, vol. 75, edited by: Laskin, A. I., Sariaslani, S., and Gadd, G. M., Advances in Applied Microbiology, 33–70, 2011.

Brown, J. R., Blankinship, J. C., Niboyet, A., van Groenigen, K. J., Dijkstra, P., Le Roux, X., Leadley, P. W., and Hungate, B. A.: Effects of multiple global change treatments on soil N_2O fluxes, Biogeochemistry, 109, 85–100, doi:10.1007/s10533-011-9655-2, 2012.

Bruemmer, C., Brueggemann, N., Butterbach-Bahl, K., Falk, U., Szarzynski, J., Vielhauer, K., Wassmann, R., and Papen, H.: Soil–atmosphere exchange of N_2O and NO in near-natural savanna and agricultural land in Burkina Faso (W. Africa), Ecosystems, 11, 582–600, doi:10.1007/s10021-008-9144-1, 2008.

Brumme, R., Borken, W., and Finke, S.: Hierarchical control on nitrous oxide emission in forest ecosystems, Global Biogeochem. Cy., 13, 1137–1148, doi:10.1029/1999gb900017, 1999.

Butterbach-Bahl, K., Baggs, E. M., Dannenmann, M., Kiese, R., and Zechmeister-Boltenstern, S.: Nitrous oxide emissions from soils: how well do we understand the processes and their controls?, Philos. T. R. Soc. B, 368, 20130122–20130122, doi:10.1098/rstb.2013.0122, 2013.

Castro, M. S., Steudler, P. A., Melillo, J. M., Aber, J. D., and Millham, S.: Exchange of N_2O and CH_4 between the atmosphere and soils in spruce-fir forests in the northeastern United-States, Biogeochemistry, 18, 119–135, doi:10.1007/bf00003273, 1992.

Cates Jr., R. L. and Keeney, D. R.: Nitrous oxide emission from native and reestablished prairies in southern Wisconsin, Am. Midl. Nat., 117, 35–42, 1987.

Chen, G. X., Huang, B., Xu, H., Zhang, Y., Huang, G. H., Yu, K. W., Hou, A. X., Du, R., Han, S. J., and VanCleemput, O.: Nitrous oxide emissions from terrestrial ecosystems in China, Chemosphere, 2, 373–378, 2000.

Ciais, P., Sabine, C., Bala, G., Bopp, L., Brovkin, V., Canadell, J., Chhabra, A., DeFries, R., Galloway, J., Heimann, M., Jones, C., Quéré, C. L., Myneni, R. B., Piao, S., and Thornton, P.: Carbon and other biogeochemical cycles, in: Climate Change 2013: The Physical Science Basis. Contribution of Working Group I to the Fifth Assessment Report of the Intergovernmental Panel on Climate Change, edited by: Stocker, T. F., Qin, D., Plattner, G.-K., Tignor, M.,

BGD
12, 3101–3143, 2015

Allen, S. K., Boschung, J., Nauels, A., Xia, Y., Bex, V., and Midgley, P. M., Cambridge University Press, Cambridge, United Kingdom and New York, NY, USA, 2013.
Collatz, G. J., Ball, J. T., Grivet, C., and Berry, J. A.: Physiological and environmental regulation of stomatal conductance, photosynthesis and transpiration: a model that includes a laminar boundary layer, Agr. Forest Meteorol., 54, 107–136, doi:10.1016/0168-1923(91)90002-8, 1991.
Collatz, G. J., Ribas-Carbo, M., and Berry, J. A.: Coupled photosynthesis-stomatal conductance model for leaves of C4 plants, Aust. J. Plant Physiol., 19, 519–538, 1992.
Davidson, E. A.: The contribution of manure and fertilizer nitrogen to atmospheric nitrous oxide since 1860, Nat. Geosci., 2, 659–662, doi:10.1038/ngeo608, 2009.
Davidson, E. A. and Trumbore, S. E.: Gas diffusivity and production of CO_2 in deep soils of the eastern Amazon, Tellus Series B-Chemical and Physical Meteorology, 47, 550–565, doi:10.1034/j.1600-0889.47.issue5.3.x, 1995.
Davidson, E. A., Nepstad, D. C., Ishida, F. Y., and Brando, P. M.: Effects of an experimental drought and recovery on soil emissions of carbon dioxide, methane, nitrous oxide, and nitric oxide in a moist tropical forest, Glob. Change Biol., 14, 2582–2590, doi:10.1111/j.1365-2486.2008.01694.x, 2008.
Dee, D. P., Uppala, S. M., Simmons, A. J., Berrisford, P., Poli, P., Kobayashi, S., Andrae, U., Balmaseda, M. A., Balsamo, G., Bauer, P., Bechtold, P., Beljaars, A. C. M., van de Berg, L., Bidlot, J., Bormann, N., Delsol, C., Dragani, R., Fuentes, M., Geer, A. J., Haimberger, L., Healy, S. B., Hersbach, H., Holm, E. V., Isaksen, L., Kallberg, P., Koehler, M., Matricardi, M., McNally, A. P., Monge-Sanz, B. M., Morcrette, J. J., Park, B. K., Peubey, C., de Rosnay, P., Tavolato, C., Thepaut, J. N., and Vitart, F.: The ERA-Interim reanalysis: configuration and performance of the data assimilation system, Q. J. Roy. Meteor. Soc., 137, 553–597, doi:10.1002/qj.828, 2011.
Del Grosso, S. J., Parton, W. J., Mosier, A. R., Ojima, D. S., Kulmala, A. E., and Phongpan, S.: General model for N_2O and N_2 gas emissions from soils due to dentrification, Global Biogeochem. Cy., 14, 1045–1060, 2000.
Dentener, F. J. and Crutzen, P. J.: A three-dimensional model of the global ammonia cycle, J. Atmos. Chem., 19, 331–369, doi:10.1007/bf00694492, 1994.
Dentener, F., Drevet, J., Lamarque, J. F., Bey, I., Eickhout, B., Fiore, A. M., Hauglustaine, D., Horowitz, L. W., Krol, M., Kulshrestha, U. C., Lawrence, M., Galy-Lacaux, C., Rast, S., Shindell, D., Stevenson, D., Van Noije, T., Atherton, C., Bell, N., Bergman, D., Butler, T., Cofala, J.,

BGD
12, 3101–3143, 2015

Collins, B., Doherty, R., Ellingsen, K., Galloway, J., Gauss, M., Montanaro, V., Mueller, J. F., Pitari, G., Rodriguez, J., Sanderson, M., Solmon, F., Strahan, S., Schultz, M., Sudo, K., Szopa, S., and Wild, O.: Nitrogen and sulfur deposition on regional and global scales: a multimodel evaluation, Global Biogeochem. Cy., 20, GB4003, doi:10.1029/2005gb002672, 2006.

Dijkstra, F. A., Prior, S. A., Runion, G. B., Torbert, H. A., Tian, H., Lu, C., and Venterea, R. T.: Effects of elevated carbon dioxide and increased temperature on methane and nitrous oxide fluxes: evidence from field experiments, Front. Ecol. Environ., 10, 520–527, doi:10.1890/120059, 2012.

Du, R., Lu, D., and Wang, G.: Diurnal, seasonal, and inter-annual variations of N_2O fluxes from native semi-arid grassland soils of inner mongolia, Soil Biol. Biochem., 38, 3474–3482, doi:10.1016/j.soilbio.2006.06.012, 2006.

Duxbury, J. M., Bouldin, D. R., Terry, R. E., and Tate, R. L.: Emissions of nitrous-oxide from soils, Nature, 298, 462–464, doi:10.1038/298462a0, 1982.

Farquhar, G. D., Caemmerer, S. V., and Berry, J. A.: A biochemical model of photosynthetic CO_2 assimilation in leaves of C_3 species, Planta, 149, 78–90, doi:10.1007/bf00386231, 1980.

Firestone, M. K. and Davidson, E. A.: Microbiological basis of NO and N_2O production and consumption in soil, in: Exchange of Trace Gases Between Terrestrial Ecosystems and the Atmosphere, edited by: Andreae, M. O. and Schimel, D. S., 7–21, 1989.

Forster, P., Ramaswamy, V., Artaxo, P., Berntsen, T., Betts, R., Fahey, D. W., Haywood, J., Lean, J., Lowe, D. C., Myhre, G., Nganga, J., Prinn, R., Raga, G., Schulz, M., and Dorland, R. V.: Changes in atmospheric constituents and in radiative forcing, in: Climate Change 2007: The Physical Science Basis. Contribution of Working Group I to the Fourth Assessment Report of the Intergovernmental Panel on Climate Change, edited by: Solomon, S., Qin, D., Manning, M., Chen, Z., Marquis, M., Averyt, K. B., Tignor, M., and Miller, H. L., Cambridge University Press, Cambridge, UK and New York, NY, USA, 2007.

Galloway, J. N., Aber, J. D., Erisman, J. W., Seitzinger, S. P., Howarth, R. W., Cowling, E. B., and Cosby, B. J.: The nitrogen cascade, Bioscience, 53, 341–356, doi:10.1641/0006-3568(2003)053[0341:tnc]2.0.co;2, 2003.

Gerber, S., Hedin, L. O., Oppenheimer, M., Pacala, S. W., and Shevliakova, E.: Nitrogen cycling and feedbacks in a global dynamic land model, Global Biogeochem. Cy., 24, GB4003, doi:10.1029/2008gb003336, 2010.

BGD
12, 3101–3143, 2015

Gerber, S., Hedin, L. O., Keel, S. G., Pacala, S. W., and Shevliakova, E.: Land use change and nitrogen feedbacks constrain the trajectory of the land carbon sink, Geophys. Res. Lett., 40, 5218–5222, doi:10.1002/grl.50957, 2013.

Goodroad, L. L. and Keeney, D. R.: Nitrous oxide emission from forest, marsh, and prairie ecosystems, J. Environ. Qual., 13, 448–452, 1984.

Groffman, P. M., Hardy, J. P., Driscoll, C. T., and Fahey, T. J.: Snow depth, soil freezing, and fluxes of carbon dioxide, nitrous oxide and methane in a northern hardwood forest, Glob. Change Biol., 12, 1748–1760, doi:10.1111/j.1365-2486.2006.01194.x, 2006.

Grover, S. P. P., Livesley, S. J., Hutley, L. B., Jamali, H., Fest, B., Beringer, J., Butterbach-Bahl, K., and Arndt, S. K.: Land use change and the impact on greenhouse gas exchange in north Australian savanna soils, Biogeosciences, 9, 423–437, doi:10.5194/bg-9-423-2012, 2012.

Guilbault, M. R. and Matthias, A. D.: Emissions of N_2O from Sonoran Desert and effluent-irrigated grass ecosytems, J. Arid Environ., 38, 87–98, doi:10.1006/jare.1997.0300, 1998.

Heinen, M.: Simplified denitrification models: overview and properties, Geoderma, 133, 444–463, doi:10.1016/j.geoderma.2005.06.010, 2006.

Henrich, M. and Haselwandter, K.: Denitrification and gaseous nitrogen losses from an acid spruce forest soil, Soil Biol. Biochem., 29, 1529–1537, doi:10.1016/s0038-0717(97)00010-2, 1997.

Hirsch, A. I., Michalak, A. M., Bruhwiler, L. M., Peters, W., Dlugokencky, E. J., and Tans, P. P.: Inverse modeling estimates of the global nitrous oxide surface flux from 1998–2001, Global Biogeochem. Cy., 20, GB1008, doi:10.1029/2004gb002443, 2006.

Ishizuka, S., Tsuruta, H., and Murdiyarso, D.: An intensive field study on CO_2, CH_4, and N_2O emissions from soils at four land-use types in Sumatra, Indonesia, Global Biogeochem. Cy., 16, GB1049, doi:10.1029/2001gb001614, 2002.

Jungkunst, H. F., Fiedler, S., and Stahr, K.: N_2O emissions of a mature Norway spruce (*Picea abies*) stand in the black forest (southwest Germany) as differentiated by the soil pattern, J. Geophys. Res.-Atmos., 109, D07302, doi:10.1029/2003jd004344, 2004.

Keller, M., Kaplan, W. A., and Wofsy, S. C.: Emissions of N_2O, CH_4 and CO_2 from tropical forest soils, J. Geophys. Res.-Atmos., 91, 1791–1802, doi:10.1029/JD091iD11p11791, 1986.

Kesik, M., Ambus, P., Baritz, R., Brüggemann, N., Butterbach-Bahl, K., Damm, M., Duyzer, J., Horváth, L., Kiese, R., Kitzler, B., Leip, A., Li, C., Pihlatie, M., Pilegaard, K., Seufert, S., Simpson, D., Skiba, U., Smiatek, G., Vesala, T., and Zechmeister-Boltenstern, S.: Invento-

BGD
12, 3101–3143, 2015

ries of N_2O and NO emissions from European forest soils, Biogeosciences, 2, 353–375, doi:10.5194/bg-2-353-2005, 2005.
Khalil, K., Mary, B., and Renault, P.: Nitrous oxide production by nitrification and denitrification in soil aggregates as affected by O_2 concentration, Soil Biol. Biochem., 36, 687–699, doi:10.1016/j.soilbio.2004.01.004, 2004.
Khalil, M. A. K., Rasmussen, R. A., French, J. R. J., and Holt, J. A.: The influence of termites on atmospheric trace gases: CH_4, CO_2, $CHCl_3$, N_2O, CO, H_2, and light-hydrocarbons, J. Geophys. Res.-Atmos., 95, 3619–3634, doi:10.1029/JD095iD04p03619, 1990.
Kitzler, B., Zechmeister-Boltenstern, S., Holtermann, C., Skiba, U., and Butterbach-Bahl, K.: Nitrogen oxides emission from two beech forests subjected to different nitrogen loads, Biogeosciences, 3, 293–310, doi:10.5194/bg-3-293-2006, 2006.
Klemedtsson, L., Klemedtsson, A. K., Moldan, F., and Weslien, P.: Nitrous oxide emission from Swedish forest soils in relation to liming and simulated increased N-deposition, Biol. Fert. Soil., 25, 290–295, doi:10.1007/s003740050317, 1997.
Koehler, B., Corre, M. D., Veldkamp, E., Wullaert, H., and Wright, S. J.: Immediate and long-term nitrogen oxide emissions from tropical forest soils exposed to elevated nitrogen input, Glob. Change Biol., 15, 2049–2066, doi:10.1111/j.1365-2486.2008.01826.x, 2009.
Li, C. S., Frolking, S., and Frolking, T. A.: A model of nitrous-oxide evolution from soil driven by rainfall events.1. model structure and sensitivity, J. Geophys. Res.-Atmos., 97, 9759–9776, 1992.
Li, C. S., Aber, J., Stange, F., Butterbach-Bahl, K., and Papen, H.: A process-oriented model of N_2O and NO emissions from forest soils: 1. Model development, J. Geophys. Res.-Atmos., 105, 4369–4384, doi:10.1029/1999jd900949, 2000.
Linn, D. M. and Doran, J. W.: Effect of water-filled pore space on carbon dioxide and nitrous oxide production in tilled and nontilled soils, Soil Sci. Soc. Am. J., 48, 1267–1272, 1984.
Luizao, F., Matson, P., Livingston, G., Luizao, R., and Vitousek, P.: Nitrous oxide flux following tropical land clearing, Global Biogeochem. Cy., 3, 281–285, doi:10.1029/GB003i003p00281, 1989.
Luo, G. J., Brüggemann, N., Wolf, B., Gasche, R., Grote, R., and Butterbach-Bahl, K.: Decadal variability of soil CO_2, NO, N_2O, and CH_4 fluxes at the Höglwald Forest, Germany, Biogeosciences, 9, 1741–1763, doi:10.5194/bg-9-1741-2012, 2012.

BGD
12, 3101–3143, 2015

Maljanen, M., Jokinen, H., Saari, A., Strommer, R., and Martikainen, P. J.: Methane and nitrous oxide fluxes, and carbon dioxide production in boreal forest soil fertilized with wood ash and nitrogen, Soil Use Manage., 22, 151–157, doi:10.1111/j.1475-2743.2006.00029.x, 2006.

Matson, A., Pennock, D., and Bedard-Haughn, A.: Methane and nitrous oxide emissions from mature forest stands in the boreal forest, Saskatchewan, Canada, Forest Ecol. Manag., 258, 1073–1083, doi:10.1016/j.foreco.2009.05.034, 2009.

Matson, P. A., Volkmann, C., Coppinger, K., and Reiners, W. A.: Annual nitrous-oxide flux and soil-nitrogen characteristics in sagebrush steppe ecosystems, Biogeochemistry, 14, 1–12, 1991.

Matson, P. A., Gower, S. T., Volkmann, C., Billow, C., and Grier, C. C.: Soil nitrogen cycling and nitrous oxide flux in a Rocky Mountain Douglas-fir forest: effects of fertilization, irrigation and carbon addition, Biogeochemistry, 18, 101–117, doi:10.1007/bf00002705, 1992.

Melling, L., Hatano, R., and Goh, K. J.: Nitrous oxide emissions from three ecosystems in tropical peatland of Sarawak, Malaysia, Soil Sci. Plant Nutr., 53, 792–805, doi:10.1111/j.1747-0765.2007.00196.x, 2007.

Milly, P. C. D. and Shmakin, A. B.: Global modeling of land water and energy balances, Part I: the land dynamics (LaD) model, J. Hydrometeorol., 3, 283–299, doi:10.1175/1525-7541(2002)003<0283:gmolwa>2.0.co;2, 2002.

Milly, P. C. D., Malyshev, S. L., Shevliakova, E., Dunne, K. A., Findell, K. L., Gleeson, T., Liang, Z., Phillipps, P., Stouffer, R. J., and Swenson, S.: An enhanced model of land water and energy for global hydrologic and earth-system studies, J. Hydrometeorol., 15, 1739–1761, 2014.

Mogge, B., Kaiser, E. A., and Munch, J. C.: Nitrous oxide emissions and denitrification N-losses from forest soils in the Bornhöved Lake region (Northern Germany), Soil Biol. Biochem., 30, 703–710, doi:10.1016/s0038-0717(97)00205-8, 1998.

Mosier, A. R., Parton, W. J., Valentine, D. W., Ojima, D. S., Schimel, D. S., and Delgado, J. A.: CH_4 and N_2O fluxes in the Colorado shortgrass steppe .1. Impact of landscape and nitrogen addition, Global Biogeochem. Cy., 10, 387–399, doi:10.1029/96gb01454, 1996.

Mummey, D. L., Smith, J. L., and Bolton, H.: Small-scale spatial and temporal variability of N_2O flux from a shrub-steppe ecosystem, Soil Biol. Biochem., 29, 1699–1706, doi:10.1016/s0038-0717(97)00077-1, 1997.

Parton, W. J., Mosier, A. R., and Schimel, D. S.: Rates and pathways of nitrous-oxide production in a shortgrass steppe, Biogeochemistry, 6, 45–58, 1988.

BGD
12, 3101–3143, 2015

Parton, W. J., Mosier, A. R., Ojima, D. S., Valentine, D. W., Schimel, D. S., Weier, K., and Kulmala, A. E.: Generalized model for N_2 and N_2O production from nitrification and denitrification, Global Biogeochem. Cy., 10, 401–412, doi:10.1029/96gb01455, 1996.

Parton, W. J., Holland, E. A., Del Grosso, S. J., Hartman, M. D., Martin, R. E., Mosier, A. R., Ojima, D. S., and Schimel, D. S.: Generalized model for NO_x and N_2O emissions from soils, J. Geophys. Res.-Atmos., 106, 17403–17419, doi:10.1029/2001jd900101, 2001.

Pei, Z. Y.: Carbon dynamics in the alpine grassland ecosystem on the tibetan plateau – a case study of wudaoliang, qinghai province, Ph.D. thesis, Institute of Geographic Sciences and Natural Resources Research, Beijing, China, 2003.

Potter, C. S. and Klooster, S. A.: Interannual variability in soil trace gas (CO_2, N_2O, NO) fluxes and analysis of controllers on regional to global scales, Global Biogeochem. Cy., 12, 621–635, doi:10.1029/98gb02425, 1998.

Potter, C. S., Matson, P. A., Vitousek, P. M., and Davidson, E. A.: Process modeling of controls on nitrogen trace gas emissions from soils worldwide, J. Geophys. Res.-Atmos., 101, 1361–1377, doi:10.1029/95jd02028, 1996.

Price, S. J., Sherlock, R. R., Kelliher, F. M., McSeveny, T. M., Tate, K. R., and Condron, L. M.: Pristine new zealand forest soil is a strong methane sink, Glob. Change Biol., 10, 16–26, doi:10.1046/j.1529-8817.2003.00710x, 2004.

Purbopuspito, J., Veldkamp, E., Brumme, R., and Murdiyarso, D.: Trace gas fluxes and nitrogen cycling along an elevation sequence of tropical montane forests in Central Sulawesi, Indonesia, Global Biogeochem. Cy., 20, GB3010, doi:10.1029/2005gb002516, 2006.

Ravishankara, A. R., Daniel, J. S., and Portmann, R. W.: Nitrous oxide (N_2O): the dominant ozone-depleting substance emitted in the 21st century, Science, 326, 123–125, doi:10.1126/science.1176985, 2009.

Rees, R. M., Wuta, M., Furley, P. A., and Li, C. S.: Nitrous oxide fluxes from savanna (miombo) woodlands in Zimbabwe, J. Biogeogr., 33, 424–437, 2005.

Rodell, M., Houser, P. R., Jambor, U., Gottschalck, J., Mitchell, K., Meng, C. J., Arsenault, K., Cosgrove, B., Radakovich, J., Bosilovich, M., Entin, J. K., Walker, J. P., Lohmann, D., and Toll, D.: The global land data assimilation system, B. Am. Meteorol. Soc., 85, 381–394, doi:10.1175/bams-85-3-381, 2004.

Rowlings, D. W., Grace, P. R., Kiese, R., and Weier, K. L.: Environmental factors controlling temporal and spatial variability in the soil–atmosphere exchange of CO_2, CH_4 and N_2O from

BGD
12, 3101–3143, 2015

an Australian subtropical rainforest, Glob. Change Biol., 18, 726–738, doi:10.1111/j.1365-2486.2011.02563.x, 2012.
Saikawa, E., Schlosser, C. A., and Prinn, R. G.: Global modeling of soil nitrous oxide emissions from natural processes, Global Biogeochem. Cy., 27, 972–989, doi:10.1002/gbc.20087, 2013.
Schiller, C. L. and Hastie, D. R.: Nitrous oxide and methane fluxes from perturbed and unperturbed boreal forest sites in northern Ontario, J. Geophys. Res.-Atmos., 101, 22767–22774, doi:10.1029/96jd01620, 1996.
Schlesinger, W. H.: On the fate of anthropogenic nitrogen, P. Natl. Acad. Sci. USA, 106, 203–208, doi:10.1073/pnas.0810193105, 2009.
Schwalm, C. R., Williams, C. A., Schaefer, K., Baker, I., Collatz, G. J., and Rödenbeck, C.: Does terrestrial drought explain global CO_2 flux anomalies induced by El Niño?, Biogeosciences, 8, 2493–2506, doi:10.5194/bg-8-2493-2011, 2011.
Seneviratne, S. I., Corti, T., Davin, E. L., Hirschi, M., Jaeger, E. B., Lehner, I., Orlowsky, B., and Teuling, A. J.: Investigating soil moisture–climate interactions in a changing climate: a review, Earth-Sci. Rev., 99, 125–161, doi:10.1016/j.earscirev.2010.02.004, 2010.
Sheffield, J., Goteti, G., and Wood, E. F.: Development of a 50 year high-resolution global dataset of meteorological forcings for land surface modeling, J. Climate, 19, 3088–3111, doi:10.1175/jcli3790.1, 2006.
Shevliakova, E., Pacala, S. W., Malyshev, S., Hurtt, G. C., Milly, P. C. D., Caspersen, J. P., Sentman, L. T., Fisk, J. P., Wirth, C., and Crevoisier, C.: Carbon cycling under 300 years of land use change: importance of the secondary vegetation sink, Global Biogeochem. Cy., 23, doi:10.1029/2007gb003176, 2009.
Simona, C., Ariangelo, D. P. R., John, G., Nina, N., Ruben, M., and Jose, S. J.: Nitrous oxide and methane fluxes from soils of the Orinoco savanna under different land uses, Glob. Change Biol., 10, 1947–1960, doi:10.1111/j.1365-2486.2004.00871.x, 2004.
Simpson, I. J., Edwards, G. C., Thurtell, G. W., den Hartog, G., Neumann, H. H., and Staebler, R. M.: Micrometeorological measurements of methane and nitrous oxide exchange above a boreal aspen forest, J. Geophys. Res.-Atmos., 102, 29331–29341, doi:10.1029/97jd03181, 1997.
Sitaula, B. K., Bakken, L. R., and Abrahamsen, G.: N-fertilization and soil acidification effects on N_2O and CO_2 emission from temperate pine forest soil, Soil Biol. Biochem., 27, 1401–1408, doi:10.1016/0038-0717(95)00078-s, 1995.

BGD
12, 3101–3143, 2015

Sousa Neto, E., Carmo, J. B., Keller, M., Martins, S. C., Alves, L. F., Vieira, S. A., Piccolo, M. C., Camargo, P., Couto, H. T. Z., Joly, C. A., and Martinelli, L. A.: Soil-atmosphere exchange of nitrous oxide, methane and carbon dioxide in a gradient of elevation in the coastal Brazilian Atlantic forest, Biogeosciences, 8, 733–742, doi:10.5194/bg-8-733-2011, 2011.

Stehfest, E. and Bouwman, L.: N_2O and NO emission from agricultural fields and soils under natural vegetation: summarizing available measurement data and modeling of global annual emissions, Nutr. Cycl. Agroecosys., 74, 207–228, doi:10.1007/s10705-006-9000-7, 2006.

Struwe, S. and Kjoller, A.: Field determination of denitrification in water-logged forest soils, FEMS Microbiol. Ecol., 62, 71–78, 1989.

Syakila, A. and Kroeze, C.: The global nitrous oxide budget revisited, Greenhouse Gas Measurement and Management, 1, 17–26, doi:10.3763/ghgmm.2010.0007, 2011.

Takakai, F., Morishita, T., Hashidoko, Y., Darung, U., Kuramochi, K., Dohong, S., Limin, S. H., and Hatano, R.: Effects of agricultural land-use change and forest fire on N_2O emission from tropical peatlands, Central Kalimantan, Indonesia, Soil Sci. Plant Nutr., 52, 662–674, doi:10.1111/j.1747-0765.2006.00084.x, 2006.

Tauchnitz, N., Brumme, R., Bernsdorf, S., and Meissner, R.: Nitrous oxide and methane fluxes of a pristine slope mire in the German National Park Harz Mountains, Plant Soil, 303, 131–138, doi:10.1007/s11104-007-9493-0, 2008.

Templer, P. H., Mack, M. C., Chapin, F. S., III, Christenson, L. M., Compton, J. E., Crook, H. D., Currie, W. S., Curtis, C. J., Dail, D. B., D'Antonio, C. M., Emmett, B. A., Epstein, H. E., Goodale, C. L., Gundersen, P., Hobbie, S. E., Holland, K., Hooper, D. U., Hungate, B. A., Lamontagne, S., Nadelhoffer, K. J., Osenberg, C. W., Perakis, S. S., Schleppi, P., Schimel, J., Schmidt, I. K., Sommerkorn, M., Spoelstra, J., Tietema, A., Wessel, W. W., and Zak, D. R.: Sinks for nitrogen inputs in terrestrial ecosystems: a meta-analysis of ^{15}N tracer field studies, Ecology, 93, 1816–1829, 2012.

Thompson, R. L., Chevallier, F., Crotwell, A. M., Dutton, G., Langenfelds, R. L., Prinn, R. G., Weiss, R. F., Tohjima, Y., Nakazawa, T., Krummel, P. B., Steele, L. P., Fraser, P., O'Doherty, S., Ishijima, K., and Aoki, S.: Nitrous oxide emissions 1999 to 2009 from a global atmospheric inversion, Atmos. Chem. Phys., 14, 1801–1817, doi:10.5194/acp-14-1801-2014, 2014.

Ullah, S. and Moore, T. R.: Biogeochemical controls on methane, nitrous oxide, and carbon dioxide fluxes from deciduous forest soils in eastern Canada, J. Geophys. Res.-Biogeo., 116, GB3010, doi:10.1029/2010jg001525, 2011.

BGD
12, 3101–3143, 2015

van Groenigen, K. J., Osenberg, C. W., and Hungate, B. A.: Increased soil emissions of potent greenhouse gases under increased atmospheric CO_2, Nature, 475, 214–216, doi:10.1038/nature10176, 2011.

Verchot, L. V., Davidson, E. A., Cattanio, J. H., Ackerman, I. L., Erickson, H. E., and Keller, M.: Land use change and biogeochemical controls of nitrogen oxide emissions from soils in eastern Amazonia, Global Biogeochem. Cy., 13, 31–46, doi:10.1029/1998gb900019, 1999.

von Arnold, K., Nilsson, M., Hanell, B., Weslien, P., and Klemedtsson, L.: Fluxes of CO_2, CH_4 and N_2O from drained organic soils in deciduous forests, Soil Biol. Biochem., 37, 1059–1071, doi:10.1016/j.soilbio.2004.11.004, 2005.

Wei, Y., Liu, S., Huntzinger, D. N., Michalak, A. M., Viovy, N., Post, W. M., Schwalm, C. R., Schaefer, K., Jacobson, A. R., Lu, C., Tian, H., Ricciuto, D. M., Cook, R. B., Mao, J., and Shi, X.: NACP MsTMIP: Global and North American Driver Data for Multi-Model Intercomparison, Data set, Oak Ridge National Laboratory Distributed Active Archive Center, Oak Ridge, Tennessee, USA, available at: http://daac.ornl.gov and doi:10.3334/ORNLDAAC/1220, 2014.

Werner, C., Butterbach-Bahl, K., Haas, E., Hickler, T., and Kiese, R.: A global inventory of N_2O emissions from tropical rainforest soils using a detailed biogeochemical model, Global Biogeochem. Cy., 21, GB3010, doi:10.1029/2006gb002909, 2007.

Wolf, K., Veldkamp, E., Homeier, J., and Martinson, G. O.: Nitrogen availability links forest productivity, soil nitrous oxide and nitric oxide fluxes of a tropical montane forest in southern Ecuador, Global Biogeochem. Cy., 25, doi:10.1029/2010gb003876, 2011.

Xu, R. and Prentice, I. C.: Terrestrial nitrogen cycle simulation with a dynamic global vegetation model, Glob. Change Biol., 14, 1745–1764, doi:10.1111/j.1365-2486.2008.01625.x, 2008.

Xu, R., Prentice, I. C., Spahni, R., and Niu, H. S.: Modelling terrestrial nitrous oxide emissions and implications for climate feedback, New Phytol., 196, 472–488, doi:10.1111/j.1469-8137.2012.04269.x, 2012.

Yu, J., Liu, J., Wang, J., Sun, W., Patrick, W. H., Jr., and Meixner, F. X.: Nitrous oxide emission from *Deyeuxia angustifolia* freshwater marsh in northeast China, Environ. Manage., 40, 613–622, doi:10.1007/s00267-006-0349-9, 2007.

Zaehle, S. and Dalmonech, D.: Carbon–nitrogen interactions on land at global scales: current understanding in modelling climate biosphere feedbacks, Curr. Opin. Environ. Sustainab., 3, 311–320, doi:10.1016/j.cosust.2011.08.008, 2011.

BGD
12, 3101–3143, 2015

Zaehle, S., Friend, A. D., Friedlingstein, P., Dentener, F., Peylin, P., and Schulz, M.: Carbon and nitrogen cycle dynamics in the O–CN land surface model: 2. Role of the nitrogen cycle in the historical terrestrial carbon balance, Global Biogeochem. Cy., 24, GB1006, doi:10.1029/2009gb003522, 2010.

Zaehle, S., Ciais, P., Friend, A. D., and Prieur, V.: Carbon benefits of anthropogenic reactive nitrogen offset by nitrous oxide emissions, Nat. Geosci., 4, 601–605, doi:10.1038/ngeo1207, 2011.

Zhuang, Q., Lu, Y., and Chen, M.: An inventory of global N_2O emissions from the soils of natural terrestrial ecosystems, Atmos. Environ., 47, 66–75, doi:10.1016/j.atmosenv.2011.11.036, 2012.

BGD
12, 3101–3143, 2015

Table A1. Texture dependent parameter k estimated from Del Grosso et al. (2000).

Soil Texture	Coarse	Medium	Fine	Coarse medium	Coarse/ fine	Medium/ fine	Coarse/ medium/ fine	Organic
k	2	10	22	6	12	16	11	2

BGD
12, 3101–3143, 2015

Table B1. Observed annual N_2O emission data for model comparison.

No	Country	Lon	Lat	Location	Veg Type	N_2O kg N ha^{-1} year^{-1}	Reference
1	Australia	133.1	−12.3	Douglas Daly region	Savanna	0.02	Grover et al. (2012)
2	Australia	148.1	−37.3	Moe	Temperate forest	0.11	Khalil et al. (1990)
3	Australia	151.9	−27.3	South-east Queensland	Tropical forest	0.52	Rowlings et al. (2012)
4	Austria	16.9	47.8	Klausenleopoldsdorf	Temperate forest	0.62	Kesik et al. (2005)
5	Austria	9.4	47.8	Achenkirch	Temperate forest	0.35	Kesik et al. (2005)
6	Austria	13.1	47.8	Innsbruck	Temperate forest	0.08	Henrich and Haselwandter (1997)
7	Austria	16.3	48.2	Schottenwald and Klausenleopoldsdorf	Temperate forest	0.76	Kitzler et al. (2006)
8	Brazil	−61.9	−2.3	Manaus	Tropical rain forest	1.9	Luizao et al. (1989)
9	Brazil	−61.9	−2.3	Manaus	Tropical rain forest	1.930	Keller et al. (1986)
10	Brazil	−54.4	−4.8	East-central Amazonia	Tropical rain forest	2.1	Davidson et al. (2008)
11	Brazil	−46.9	−2.3	Paragominas	Rainforest	2.430	Verchot et al. (1999)
12	Burkina Faso	−1.9	10.3	Ioba	Savanna	0.6	Bruemmer et al. (2008)
13	Canada	−80.6	50.3	Ontario	Boreal forest	0.04	Schiller and Hastie (1996)
14	Canada	−106.9	52.8	Saskatchewan	Boreal forest	0.28	Simpson et al. (1997)
15	Canada	−103.1	52.8	Saskatchewan	Boreal forest	0.07	Matson et al. (2009)
16	Canada	−106.9	52.8	Saskatchewan	Boreal forest	0.09	Matson et al. (2009)
17	Canada	−73.1	45.3	Mont St. Hilaire	Temperate forest	0.42	Ullah and Moore (2011)
18	China	91.9	35.3	Tibet	Alpine grassland	0.07	Pei (2003)
19	China	125.6	40.3	Changbai mountain	Alpine tundra, temperate forest	0.56	Chen et al. (2000)
20	China	114.4	42.8	Inner mongolia	Temperate forest	0.73	Du et al. (2006)
22	China	133.1	47.8	Sanjiang Experimental Station	Freshwater marshes	0.21	Yu et al. (2007)
23	Denmark	13.1	55.3	Solo	Temperate forest	0.29	Kesik et al. (2005)
24	Denmark	13.1	55.3	Denmark	Temperate forest	0.52	Struwe and Kjoller (1989)
25	Ecuador	−80.6	−4.8	Bombuscaro	Tropical forest	0.3	Wolf et al. (2011)
26	Finland	24.4	60.3	Southern	Boreal forest	0.78	Maljanen et al. (2006)
27	Germany	9.4	50.3	Average	Temperate forest	0.57	Templer et al. (2012)
28	Germany	9.4	52.8	Kiel	Temperate forest	0.4	Mogge et al. (1998)
29	Germany	9.4	47.8	Southwest	Temperate forest	0.93	Jungkunst et al. (2004)
30	Germany	13.1	47.8	Höglwald	Temperate forest	0.41	Luo et al. (2012)
31	Germany	9.4	52.8	Average	Temperate forest	0.66	Brumme et al. (1999)
32	Germany	9.4	52.8	Harz mountains	Mire	0.25	Tauchnitz et al. (2008)
34	Indonesia	103.1	−2.3	Jambi	Lowland tropical rainforest	0.260	Ishizuka et al. (2002)
35	Indonesia	121.9	−2.3	Central Sulawesi	Tropical seasonal rain forest	0.800	Purbopuspito et al. (2006)
36	Indonesia	114.4	−2.3	Central Kalimantan	Tropical forest	2.51	Takakai et al. (2006)
37	Italy	9.4	45.3	P.Ticino BoscoNegri	Temperate forest	0.18	Kesik et al. (2005)
38	Malaysia	110.6	−2.3	Sarawak	Mixed peat swamp forest	0.7	Melling et al. (2007)
39	New Zealand	170.6	−44.8	New Zealand	Temperate forest	0.01	Price et al. (2004)
40	Norway	9.4	60.3	Norway	Temperate forest	0.73	Sitaula et al. (1995)
41	Panama	−80.6	7.8	Gigante Peninsula	Tropical forests	1.6	Koehler et al. (2009)
42	Sweden	13.1	57.8	Southwestern	Temperate forest	0.07	Klemedtsson et al. (1997)
43	Sweden	13.1	57.8	Asa experimental forest	Undrained bog	0.65	von Arnold et al. (2005)
44	UK	−1.9	55.3	Northumberland	Grassland	0.3	Ball et al. (2007)
45	USA	−73.1	42.8	Harvard forest	Mixed hardwood	0.04	Bowden et al. (1990)
46	USA	−73.1	40.3	New York	Temperate forest	0.9	Duxbury et al. (1982)
47	USA	−80.6	25.3	Florida	Marsh	1	Duxbury et al. (1982)
48	USA	−73.1	42.8	New Hampshire	Temperate forest	0.070	Groffman et al. (2006)
49	USA	−106.9	35.3	New mexico	Temperate forest	0.06	Matson et al. (1992)
50	USA	−118.1	45.3	Washington	Temperate shrub-steppe	0.15	Mummey et al. (1997)
51	USA	−114.4	37.8	Mojave desert	Perennial grasses	0.11	Billings et al. (2002)
52	USA	−106.9	40.3	Wyoming	Sagebrush steppe	0.21	Matson et al. (1991)
53	USA	−73.1	45.3	Northeastern	Temperate forest	0.18	Castro et al. (1992)
54	USA	−69.4	45.3	Northeastern	Temperate forest	0.03	Castro et al. (1992)
55	USA	−103.1	40.3	Colorado	Temperate steppe	0.14	Mosier et al. (1996)
56	USA	−88.1	42.8	Wisconsin	Grass	0.040	Cates and Keeney (1987)
57	USA	−114.4	37.8	Nevada	Mojave desert	0.11	Billings et al. (2002)
58	USA	−110.6	32.8	Arizona	Sonoran desert	0.4	Guilbault and Matthias (1998)
59	USA	−118.1	45.3	Ft. Collins, Colorado	Temperate grassland	0.12	Parton et al. (1988)
60	Venezuela	−61.9	10.3	Venezuela	Savana	0.73	Simona et al. (2004)
61	Zimbabwe	31.9	−17.3	Harare	Miombo woodland savanna	0.51	Rees et al. (2005)

BGD
12, 3101–3143, 2015

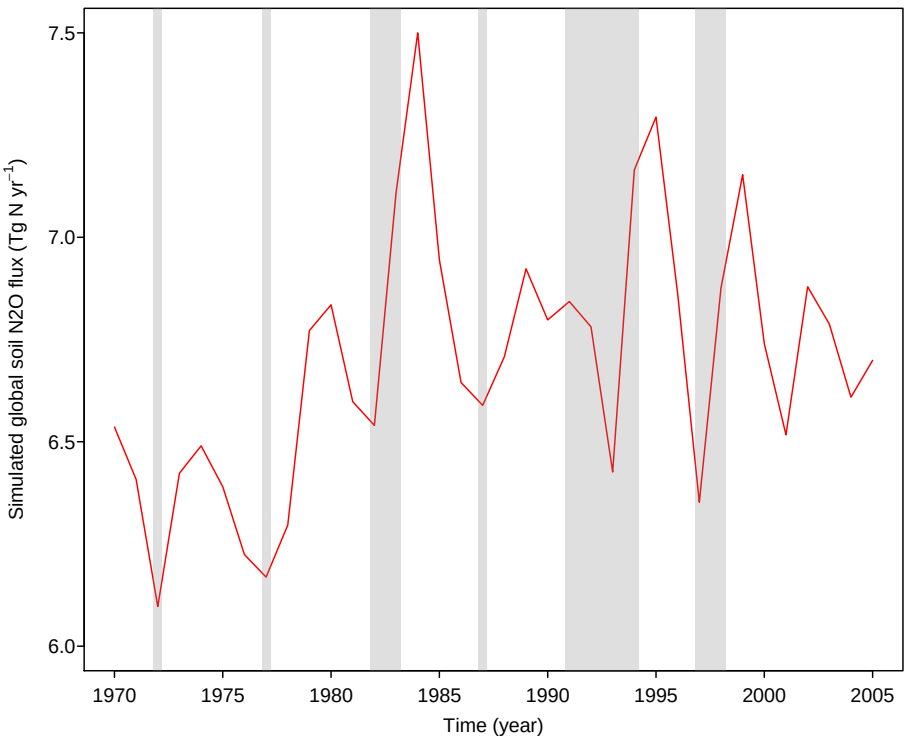

Figure 1. Simulated annual global soil N_2O emissions based on potential vegetation (1970–2005). Shaded grey area indicates El Niño years with the multivariate ENSO index (MEI) greater than 0.6.

BGD
12, 3101–3143, 2015

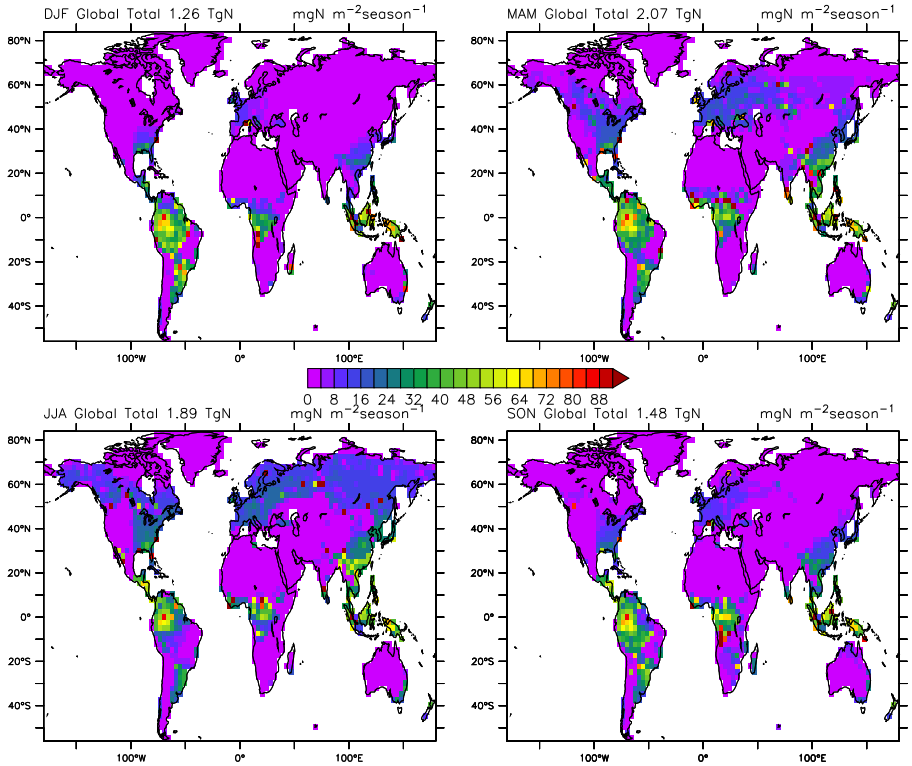

Figure 2. Global seasonal mean soil N_2O emissions (with potential vegetation) averaged over the years 1970–2005. DJF (December, January and February), stands for Northern Hemisphere Winter; MAM (March, April and May) for Spring; JJA (June, July and August) for Summer; and SON (September, October and November) for Autumn.

BGD
12, 3101–3143, 2015

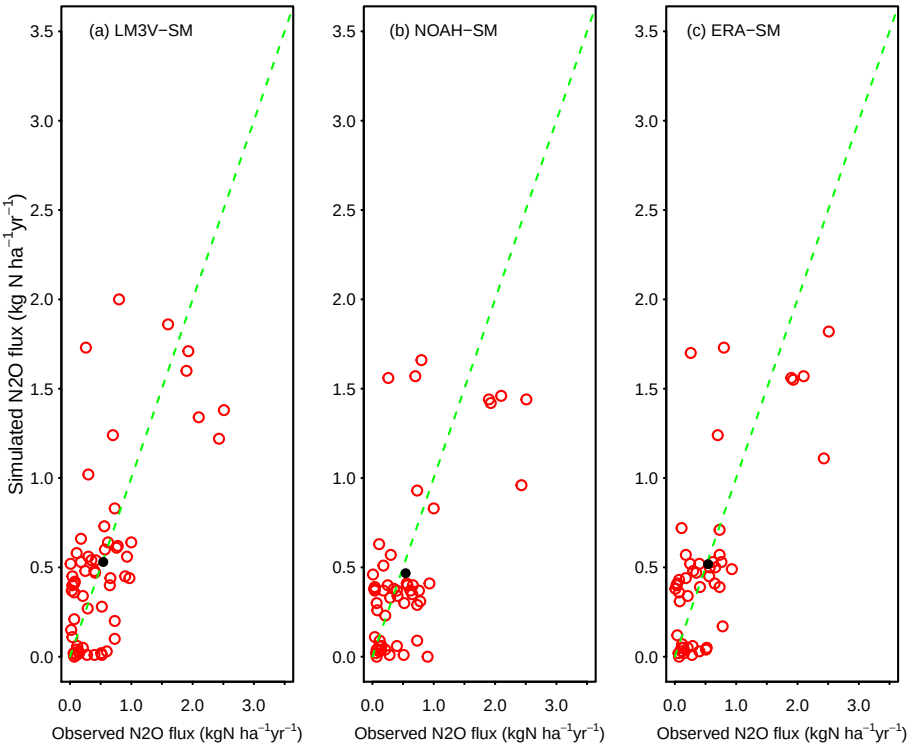

Figure 3. Observed vs. simulated annual N_2O emissions from natural soils. Dashed green lines are the 1 : 1 lines. The solid circles represent the overall means. Different panels represent simulations with different soil moisture data: **(a)** LM3V-SM (simulated by LM3V-N); **(b)** NOAH-SM (based on land surface model NOAH 3.3 in Global Land Data Assimilation System Version 2); and **(c)** ERA-SM (reanalysis data from ECMWF). Water filled pore space (WFPS) is calculated using the average of the one based on available water capacity and the one based on the total porosity (Method 3, see the main text for detailed description) for panel **(a)**; and using the total porosity (Method 2) for panel **(b)** and **(c)**.

BGD
12, 3101–3143, 2015

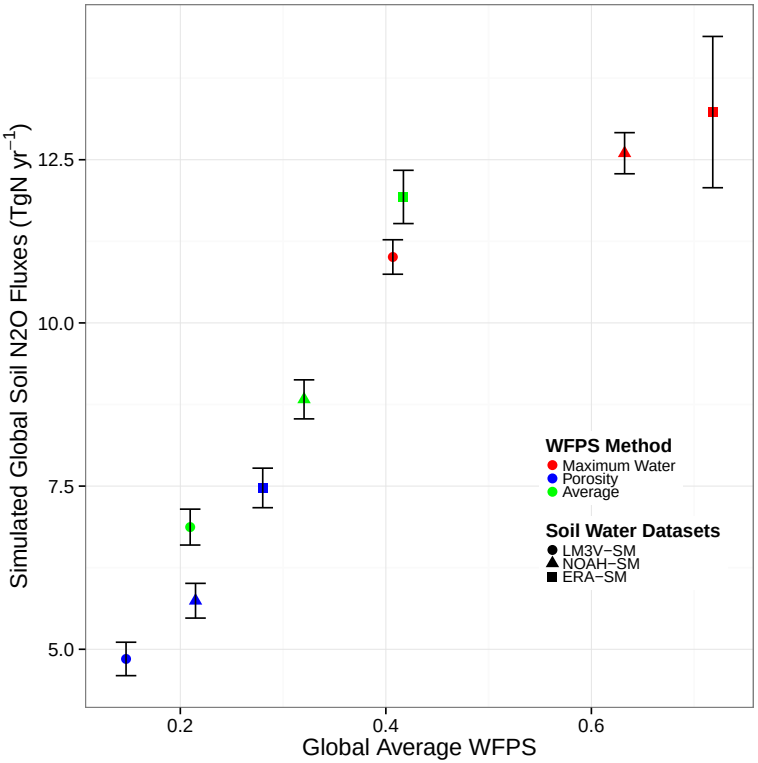

Figure 4. Sensitivity of simulated global soil N_2O emissions (with potential vegetation) to water filled pore space (WFPS). The *x* axis is the WFPS averaged globally over 1982–2005; the *y* axis represents the corresponding global total N_2O fluxes. A total of nine sets of WFPS are obtained through either different soil water datasets (colours) or varied calculation methods (symbols). Coloured symbols represent interannual means and error bars indicate interannual SDs.

BGD
12, 3101–3143, 2015

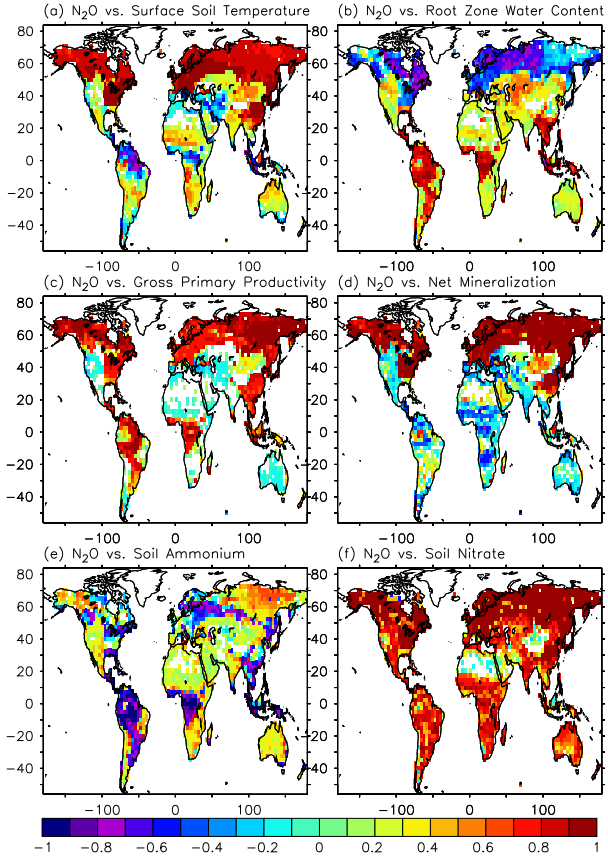

Figure 5. Temporal correlations between simulated monthly natural soil N_2O emissions and **(a)** surface soil temperature, **(b)** root zone water content, **(c)** gross primary productivity, **(d)** net mineralization, **(e)** soil ammonium, and **(f)** soil nitrate. White areas in panel **(a)** to **(f)** indicate locations either with no data or no significant ($\alpha > 0.05$) Pearson correlation coefficients.

BGD
12, 3101–3143, 2015

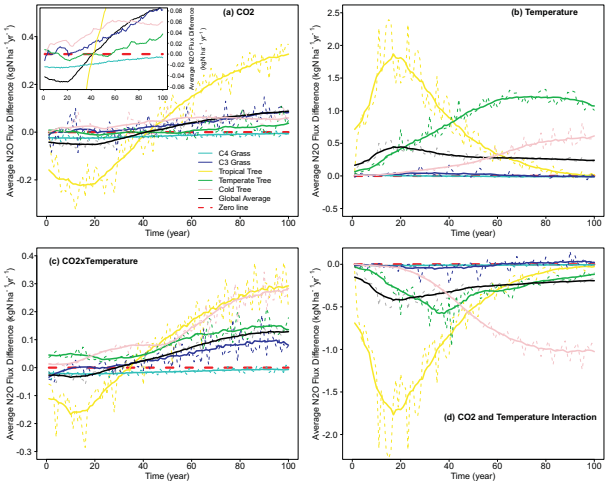

Figure 6. Soil N_2O emissions in response to step increases in atmospheric CO_2 and temperature. Panel **(a)** is the response to CO_2 fertilization alone, expressed as the difference between CO_2 increased run and the control run (CO2_FERT – CONTROL), the inset zooms into the *y* axis (flux difference) around zero; Panel **(b)** is the response to temperature increase alone (TEMP-CONTROL); Panel **(c)** is the combined response to both CO_2 enrichment and temperature rise (CO2_FERT × TEMP-CONTROL); and Panel **(d)** is the interactive effect of CO_2 and temperature responses, which is the difference between the combined (results from Panel **(c)**) and minus the individual responses (results from Panel **(a)** and **(b)**). Results are shown as annual values (thin dashed lines) and as running average with a moving window of 17 years (period of recycled climate forcing, thick solid lines). The black lines represent the global average response. Coloured lines indicate responses for biome as represented by each plant functional type (PFT) considered in LM3V-N: C4 grass (cyan), C3 grass (blue), tropical forest (yellow), temperate deciduous forest (green) and cold evergreen forest (pink). Dashed red line represents the zero line.

BGD
12, 3101–3143, 2015